Title: A Paracrine-to-Autocrine Shunt of GREM1 Fuels Colorectal Cancer Metastasis via ACVR1C

Huaixiang Zhou[1,]†, Qunlong Jin[1,2,]†, Zhang Fu[1,]†, Yanming Yang[1,]†, Yunfei Gao[1], Niu Wang[3], Bo Zhao[3], Long Gui[4], Jiang Li[5], Zijing Zhu[6], Ying Zhang[1], Yulong He[2], Ying Zhang[7], Shouqing Luo[8], Li Fu[9], Xudong Wu[10], Junjing Zhang[11], Xuetong Shen[12,]*, Tao Wang[1,]* , Youheng Jiang[1,2,] *, and Ningning Li[1,11,]*

Affiliations

[1] Tomas Lindahl Nobel Laureate Laboratory, The Seventh Affiliated Hospital, Sun Yat-sen University, Shenzhen, China

[2] Digestive Diseases Center, Guangdong Provincial Key Laboratory of Digestive Cancer Research, The Seventh Affiliated Hospital of Sun Yat-sen University, Shenzhen, China

[3] School of Medicine, Shenzhen Campus of Sun Yat-sen University, Shenzhen, China

[4] Institute of Bio-Architecture and Bio-Interactions, Shenzhen Medical Academy of Research and Translation, Shenzhen, China

[5] Clinical Big Data Research Center, The Seventh Affiliated Hospital of Sun Yat-sen University, Shenzhen, China

[6] Key Laboratory of Epigenetic Regulation and Intervention, Institute of Biophysics, Chinese Academy of Sciences, Beijing, China

[7] The Francis Crick Institute, London, UK

[8] Peninsula Medical School, Faculty of Health, University of Plymouth, Plymouth, UK

[9] Guangdong Key Laboratory for Genome Stability & Disease Prevention, Department of Pharmacology and Shenzhen International Cancer Center, Shenzhen University Medical School, Shenzhen University, Shenzhen, China

[10] The Province and Ministry Co-sponsored Collaborative Innovation Center for Medical Epigenetics, Key Laboratory of Immune Microenvironment and Disease (Ministry of Education), Department of Cell Biology, School of Basic Medical Sciences, Tianjin Medical University, Tianjin, China

[11] Hohhot Key Laboratory of Tumor Biology and Precision Medicine, Hohhot First Hospital, Hohhot, China

[12] Institute of Cancer Research, Shenzhen Bay Laboratory, Shenzhen, China

† These authors contributed equally

* Corresponding author:
Ningning Li, lead contact
Email: linn29@mail.sysu.edu.cn
Youheng Jiang
Email: jiangyouheng1@sysush.com
Tao Wang

Email: wangtao@sysush.com
Xuetong Shen
Email: snowshen@mac.com

Abstract

Tumor cells typically rely on paracrine stromal signals to guide malignant behaviors, but whether they acquire signaling autonomy to support metastasis remains unclear. We elucidate this in colorectal cancer (CRC) by uncovering a paracrine-to-autocrine shunt of Gremlin1 (GREM1), a canonical stromal-secreted antagonist of bone morphogenetic proteins (BMPs). We demonstrate that while GREM1 remains restricted to stromal cells in earlier-stage (I–III) CRC, its ectopic expression in tumor epithelium increases markedly in stage IV. Mechanistically, we identify ACVR1C as a novel, high-affinity epithelial receptor for GREM1. Their interaction activates SMAD2/3 signaling, which upregulates *SNAI1* and *GREM1*, establishing a feedback loop that amplifies epithelial-mesenchymal transition (EMT). Disrupting this loop impairs CRC metastasis *in vivo*. Clinically, epithelial GREM1 or ACVR1C expression predicts metastasis and poor survival. These findings define a paradigm in which tumor cells hijack stromal GREM1 to establish a GREM1–ACVR1C autocrine loop that sustains EMT and metastasis, marking a shift toward signaling autonomy and revealing a targetable vulnerability in advanced CRC.

Introduction

Distant metastasis remains the leading cause of death in colorectal cancer (CRC) patients(*1*). Epithelial–mesenchymal transition (EMT) is recognized as a critical early event initiating the metastatic cascade(*2*). A complex interplay exists between tumor epithelial cells and various non-malignant components of the tumor microenvironment (TME), including cancer-associated fibroblasts (CAFs) and immune cells. This dynamic interaction is considered one of the central drivers of tumor initiation, progression, and phenotypic plasticity(*3*). Among these interactions, stroma-derived cytokines and chemokines help sustain the malignant phenotypes of tumor cells via paracrine signaling(*4-6*). However, as tumor cells detach from the primary site to metastasize, they inevitably lose continuous support from the local TME—including stromal cells, extracellular matrix components, and localized signaling cues. Although tumor cells may, in certain contexts, co-migrate with CAFs and microenvironmental fragments into the circulation, the support they retain remains significantly limited compared to that at the primary site(*7*). Nonetheless, the support from these co-migrating components remains extremely limited compared to the primary site. This abrupt interruption of paracrine support is considered a major bottleneck that restricts the majority of tumor cells from successfully establishing distant colonies, with only a minority capable of seeding metastases eventually(*8*).

As such, this phenomenon raises a fundamental yet unresolved question: how do a small subset of tumor cells maintain metastasis-associated phenotypes without sustained microenvironmental paracrine support? Given the extensive cross-talk between tumor cells and the TME, these metastasis-competent cells may have already undergone profound remodeling of their intrinsic properties via prolonged and dynamic interactions with TME at the primary site. This ability to sustain malignant behavior without external cues can be viewed as a form of ‘signaling autonomy,’ echoing the classic cancer hallmark of “self-sufficiency in growth signals” described by Hanahan and Weinberg(*9*). This hallmark refers to the ability of tumor cells to produce their own growth factors via autocrine loops, thereby bypassing the need for exogenous mitogenic stimulation and maintaining persistent signaling. While signaling autonomy has been extensively explored in the context of proliferation and survival, it is crucial to determine whether metastasizing tumor cells can achieve autonomous control over the programs that sustain EMT and migratory behavior—a capacity that could serve as an intrinsic driver of successful metastasis.

Within the TME, CAFs represent one of the most active stromal components and play essential roles in tumor initiation and progression through bidirectional interactions with cancer cells(*10*, *11*). Notably, within the highly heterogeneous CAF population(*12*), a GREM1-expressing subset has attracted increasing attention. Several studies have demonstrated that GREM1 CAFs promote tumor progression via the paracrine secretion of GREM1 in both CRC(*13-15*) and breast cancer(*16*).

Intriguingly, recent evidence indicates that GREM1 expression is not restricted to stromal CAFs. In pancreatic(*17*) and prostate cancers(*18*), tumor epithelial cells have been shown to express and secrete GREM1, regulating their own phenotypic plasticity. Similarly, in Hereditary Mixed Polyposis Syndrome (HMPS), epithelial-specific upregulation of GREM1 is markedly enhanced in intestinal tissue(*19*). Nonetheless, whether epithelial GREM1 expression occurs in sporadic CRC patients remains unclear, and its potential role in promoting cancer cell plasticity and metastasis has yet to be determined. Studies, including ours, have shown that modulating GREM1 expression in CRC cell lines can affect cell migration and EMT-related phenotypes(*20, 21*). Yet, whether CRC epithelial cells can "hijack" stromal GREM1 signals to ultimately activate their own GREM1 expression for malignant progression remains an open question. Mechanistically, GREM1 was initially identified as a canonical antagonist of the bone morphogenetic protein (BMP) signaling pathway(*22*). Considering that BMPs are ligands rather than receptors and thus less likely to directly mediate GREM1's potential autocrine function, it becomes critical to identify potential GREM1 receptors on CRC cells. Recent studies indicate that GREM1 also possesses cytokine-like functions, capable of binding to several noncanonical receptors, including VEGFR2(*23*), FGFR1(*18*), and EGFR(*24*), suggesting that it may influence cancer cell behavior through multiple signaling routes. However, it remains unclear whether GREM1 mediates its signaling autonomy during CRC progression via previously reported noncanonical receptors or other yet-to-be-identified ones.

This study aims to address two fundamental issues related to GREM1 signaling in CRC metastasis. First, we investigate whether CRC epithelial cells can acquire autonomous GREM1 signaling during tumor progression. Second, we examine whether GREM1 can regulate EMT and metastatic phenotypes through noncanonical receptors in CRC. By systematically elucidating how GREM1 signaling in CRC may undergo a paracrine-to-autocrine shunt, we seek to uncover a novel mechanism conferring signaling autonomy and metastatic competence. In doing so, our study positions GREM1 as an exemplar within a broader conceptual framework of metastasis wherein acquiring signaling autonomy is a critical driver of advanced progression. These efforts may not only provide a new paradigm for understanding how signaling autonomy contributes to metastasis but also establish a theoretical foundation for targeting the GREM1 signaling axis as a new anti-metastatic strategy.

Ectopic expression of GREM1 during CRC progression

In the gut, GREM1 marks a subpopulation of fibroblasts in both normal(*25*) and tumor tissues(*13*). Using *Grem1-CreER^{T2};Rosa-mTmG* mice(*25*), we confirmed that Grem1^{+} cells are exclusively confined to the stromal compartment, and distributed along the intestinal isthmus and adjacent to α-SMA^{+} myofibroblasts(*26*), two months post-tamoxifen (TMX) injection (Fig. S1A–C). Extending this observation to humans, we found that GREM1 was likewise absent from epithelial cells in normal intestinal

tissues, but sporadically expressed in stromal cells (Fig. S1D), suggesting a conserved stromal specificity. Similarly, in human stage I-III CRC samples, GREM1 staining co-localized with VIMENTIN (VIM, a stromal cell marker, encoded by *VIM*)(*26*, *27*) and fibroblast activation protein (FAP, an activated fibroblast marker)(*26*), but was mutually exclusive with β-CATENIN (β-CAT, a CRC cell marker, encoded by *CTNNB1*)(*28*), CD68 (a macrophage marker)(*27*), or α-SMA (a myofibroblast marker) (Fig. S1E–J). These findings confirm that GREM1 is a bona fide stromal factor and $GREM1^{+}$ stromal cells are a subtype of cancer-associated fibroblasts (CAFs), potentially contributing to CRC progression(*13*, *15*).

To systematically investigate the distribution and clinical significance of GREM1, we first performed immunohistochemical (IHC) staining on 106 human primary CRC samples spanning all four stages. We observed a stage-dependent redistribution of GREM1 cells: in early-stage tumors (stage I–II), GREM1 stromal cells were predominantly restricted to the peritumoral stroma; in stage III, these cells more frequently infiltrated the tumor parenchyma; in stage IV, infiltration of GREM1 stromal cells showed a decreasing trend (with no statistically significant difference compared to stage III). Notably, in stage IV tumors, strong GREM1 staining emerged in a subset of tumor epithelial regions (Fig. 1A–C). These findings suggest a potential shift of GREM1 expression from stroma to epithelium during tumor progression.

To dissect the cellular sources and stage-specific dynamics of GREM1 expression at higher resolution, we analyzed publicly available single-cell RNA sequencing (scRNA-seq) datasets covering CRC samples from stages I–IV. Consistent with IHC data, GREM1 expression was primarily detected in fibroblasts and epithelial cells (Fig. S2A–C). Stage-specific analysis revealed a marked upregulation of GREM1 in fibroblasts at stages III and IV (Fig. S2D). Strikingly, GREM1 epithelial cells were detected almost exclusively in stage IV tumors (Fig. S2E), supporting the notion that ectopic GREM1 expression by tumor cells is a late event in CRC progression. This observation was further validated by colocalization of GREM1 with an epithelial marker epithelial cell adhesion molecule (EPCAM)(*27*) in tumor cells (Fig. 1D). Finally, survival analysis demonstrated that patients with high GREM1 expression in tumor cells had significantly shorter overall survival compared to those with low expression (Fig. 1E). Taken together, these results reveal that while GREM1 CAFs are present throughout CRC progression, GREM1 tumor epithelial cells emerge predominantly in advanced CRC, indicating that GREM1 expression, initially restricted to stromal cells, is progressively co-opted by tumor epithelial cells as CRC advances.

ACVR1C is a novel GREM1 receptor in CRC

This spatiotemporal ectopic expression of GREM1 suggests that tumoral autocrine signaling may be initiated by preceding stromal paracrine cues. Given the potential

for intercellular communication mediated by the infiltration of GREM1 stromal cells into the tumor parenchyma, we hypothesized that CRC tumor cells might express GREM1 receptor(s), through which downstream signaling cascades drive tumoral GREM1 expression and promote CRC progression. To identify potential GREM1 receptors, we overexpressed HA-tagged GREM1 in the human CRC cell line HCT116 (Fig. 2A). Mass spectrometry analysis of proteins pulled down using anti-HA beads identified activin A receptor type 1C (ACVR1C), a member of the TGFβ superfamily, as a potential GREM1 receptor (Fig. 2B, Fig. S3A).

To validate this interaction, we performed co-immunoprecipitation (co-IP) assays using HA-tagged GREM1 in HCT116 cells. Immunoblotting revealed that GREM1 interacted with ACVR1C specifically, while no such interaction was detected with other members of the TGFβ superfamily such as TGFβR1 (Fig. 2C). Similarly, co-IP assays using Flag-tagged ACVR1C confirmed the interaction with GREM1, which was abolished by a GREM1-blocking antibody (BAb) (Fig. 2D). Confocal microscopy revealed the co-localization of ACVR1C with GREM1 in SW480 CRC cells (Fig. 2E). We next examined whether a direct interaction exists between GREM1 and ACVR1C. We found that Fc-tagged ACVR1C extracellular domain (ACVR1C-ECD, $AA_{1\text{-}113}$) and His-tagged full-length GREM1 were pulled down together, demonstrating a direct physical association between ACVR1C and GREM1 (Fig. 2F). Further analysis of the binding affinity of GREM1 for ACVR1C using microscale thermophoresis (MST) revealed that ACVR1C-ECD exhibited a 12.6-fold higher affinity for GREM1 (K_d = 67.67 ± 10.35 nM) than that for ACTIVIN B (K_d = 854.1 ± 127.47 nM), a known ligand of ACVR1C(*29*) (Fig. 2G).

To further delineate the explicit interaction mode of GREM1 and ACVR1C, we constructed truncated GREM1 and ACVR1C-ECD. Co-IP assays showed that deletion of amino acids 100–157 ($AA_{100–157}$) in GREM1 or 68–113 ($AA_{68–113}$) in ACVR1C-ECD effectively abolished their interaction in HCT116 cells (Fig. 2H, I). Based on these findings, we aimed to identify key residues mediating the interaction between GREM1 and ACVR1C. The HDOCK platform (http://hdock.phys.hust.edu.cn/) was utilized to simulate potential docking modalities between GREM1 (PDB: 5AEJ)(*30*) and ACVR1C (AlphaFold prediction, https://alphafold.ebi.ac.uk/entry/Q8NER5) based on their structures. Residues Q101/T102/T112/N115 in GREM1 and Q72/E85/T101 in ACVR1C were predicted to be essential for binding (Fig. 2J). To validate, we performed site-directed mutagenesis of the predicted residues to assess binding. Notably, the Q101A/T102A/T112A/N115A quadruple mutation in GREM1, or single mutations E85A or T101A in ACVR1C, significantly abrogated the GREM1-ACVR1C interaction (Fig. 2K, L). Further, we found no detectable interaction between recombinant GREM1 and the ACVR1C-ECD double mutant (E85A/T101A) by assessing their binding affinity using MST (Fig. S3B). These data suggest that Q101/T102/T112/N115 in GREM1, and E85/T101 in ACVR1C are key residues mediating their interaction. Clinically, IHC and scRNA-seq revealed that ACVR1C is

expressed in tumor cells, with markedly elevated levels in stage IV CRC (Fig. S3C–E). Notably, high ACVR1C expression correlates with poor prognosis in stage IV CRC patients, supporting ACVR1C's tumor-promoting role and consistent with the clinical significance of GREM1 (Fig. S3F). Taken together, these results demonstrate that ACVR1C is a novel receptor of GREM1 in CRC.

Secretory GREM1 induces EMT via the ACVR1C-SMAD2/3 pathway but not TGFβR/BMPR pathways

To explore whether GREM1 serves as a functional ligand for ACVR1C in CRC cells, we first generated GREM1-enriched conditioned medium (GREM1-CM) and control conditioned medium (Vec-CM) using HEK293 cells (Fig. S4A–C). We then performed RNA-sequencing (RNA-seq) on HCT116 cells treated with GREM1-CM or Vec-CM. Gene Set Enrichment Analysis (GSEA) revealed that SMAD2/3 and EMT pathways were significantly enriched in CRC cells treated with GREM1-CM (Fig. 3A). ACVR1C is one of the receptors of the TGFβ superfamily, and it transduces signals primarily through the phosphorylation of SMAD2/3 (p-SMAD2/3)(*31*). Since commercial antibody for phosphorylated ACVR1C is not available, detection of p-SMAD2/3 serves as an effective proxy to reflect ACVR1C-SMAD2/3 activation. To confirm the effect of secretory GREM1 on the ACVR1C-SMAD2/3 pathway and EMT in CRC cells, we performed immunoblotting and found that GREM1-CM significantly increased p-SMAD2/3 levels in HCT116 and SW480 cells, which was effectively blocked by a GREM1 BAb (Fig. 3B). Moreover, immunoblotting and RT–qPCR analyses also revealed that GREM1-CM induced significant downregulation of E-CADHERIN (E-CAD, encoded by *CDH1*)(*32*) and upregulation of mesenchymal markers, including SNAIL (encoded by *SNAI1*), ZEB1, and β-CAT(*28*, *33*) in SW480 and HCT116 cells. GREM1 BAb effectively blocked GREM1-CM-induced EMT activation (Fig. 3B and Fig. S4D, E). Considering that EMT serves as an effective mechanism through which tumor cells acquire stroma-like traits to promote invasion and metastasis, we tested whether blocking GREM1 could inhibit the invasive and migratory capacity of CRC cells. Indeed, *in vitro* scratch and transwell assays showed that GREM1-CM significantly enhanced migration and invasion abilities of HCT116 and SW480 cells. Remarkably, these effects were abolished by GREM1 BAb treatment (Fig. S4F–I). These findings suggest that secretory GREM1 activates the ACVR1C-SMAD2/3 pathway and promotes EMT and subsequent cellular behavior, such as migration and invasion of CRC cells.

The TGFβ superfamily signals through BMPRs, ACVRs, and TGFβRs. Although both ACVRs and TGFβRs converge on the SMAD2/3 axis(*31*), and GREM1-CM robustly activated TGFβ superfamily signaling in HEK293 cells (Fig. S4J), our co-IP analysis showed no direct interaction between GREM1 and TGFβR1 (Fig. 2C). To determine whether GREM1 activates SMAD2/3 via TGFβR1 or ACVR1C, we treated SW480 and HCT116 cells with increasing concentrations of recombinant human

GREM1 (rhGREM1). This led to a dose-dependent increase in p-SMAD2/3 (Fig. 3C), suggesting activation of a SMAD2/3-coupled receptor. To exclude the possibility that GREM1 indirectly stimulates TGFβ signaling, we examined whether rhGREM1 alters the expression of TGFβ or TGFβR1 in CRC cells. No changes were observed across all doses tested (Fig. 3C), indicating that GREM1 does not upregulate endogenous TGFβ signaling components. Together, these data suggest that GREM1-induced SMAD2/3 activation is unlikely to be mediated by TGFβR1 and instead proceeds via the ACVR1C pathway (Fig. 3D).

Considering that GREM1 is a canonical antagonist of BMP and that BMP receptors (BMPRs) exert their function through the phosphorylation of SMAD1/5/9 (p-SMAD1/5/9), we sought to investigate whether GREM1 regulates EMT via BMPR superfamily pathways. As expected, rhGREM1 suppressed the p-SMAD1/5/9 (Fig. 3C), in keeping with the canonical role of GREM1 as a BMP inhibitor. However, rescue of BMP signaling using the specific agonist sb4, which exclusively increases p-SMAD1/5/9 levels without affecting p-SMAD2/3(*34*), failed to reverse GREM1-induced EMT marker changes (Fig. 3E). This definitive exclusion of BMPR-SMAD1/5/9 involvement establishes that GREM1 promotes EMT independently of its classical role as a BMP inhibitor.

Subsequently, to examine whether GREM1 promotes EMT through activation of the ACVR1C-SMAD2/3 pathway, we either stably knocked down ACVR1C (shACVR1C) or inhibited SMAD2/3 phosphorylation using SB505124(*35*). Our immunoblotting and RT–qPCR analysis revealed that shACVR1C or SB505124 significantly blocked GREM1-CM-induced changes in EMT marker expression (*i.e.* E-CAD, ZEB1, β-CAT and SNAIL), indicating that ACVR1C-SMAD2/3 activation is required for GREM1-driven EMT in SW480 and HCT116 CRC cells (Fig. 3F, g and Fig. S5A, B and 6A, B). In addition, GREM1-CM-induced invasion and migration of these CRC cells was abolished by shACVR1C or SB505124 (Fig. S5C–G and 6C–F). Collectively, these findings demonstrate that GREM1 induces EMT, as well as subsequent migration and invasion, by activating the ACVR1C-SMAD2/3 pathway.

p-SMAD2/3 form a complex with SMAD4 that translocates into the nucleus and acts as a transcriptional regulator(*36*). *SNAI1* has been identified as a transcriptional target of the SMAD2/3/4 complex in several cancers, including CRC(*37-39*). To define the direct binding sites involved in this regulation in CRC cells, we queried the JASPAR database (http://jaspar.genereg.net/) and identified three candidate SMAD2/3/4 binding sites (–967, –787, and –186) within the *SNAI1* promoter (Fig. S6G). Chromatin immunoprecipitation (ChIP) followed by qPCR confirmed specific binding of SMAD2/3/4 to the –787 site. Importantly, inhibition of ACVR1C with SB505124 significantly decreased this binding (Fig. S6H). Overall, our data reveal that secretory GREM1 is a specific functional ligand that activates the ACVR1C–

SMAD2/3–SNAIL signaling axis, thereby promoting EMT, invasion and migration of CRC cells.

Exogenous GREM1 induction of endogenous *GREM1* transcription reinforces EMT in CRC cells via the ACVR1C-SMAD2/3 pathway

Our data above show that there is a marked increase in the proportion of GREM1$^+$ epithelial tumor cells in stage IV CRC (Fig. 1C and Fig. S2E). To determine whether exogenous GREM1 can regulate endogenous GREM1 expression, we treated SW480 cells with increasing concentrations of rhGREM1. RT-qPCR and immunoblotting analyses revealed a dose-dependent upregulation of tumor GREM1 expression in response to rhGREM1 stimulation (Fig. 4A–C). However, the mechanism by which exogenous GREM1 triggers endogenous *GREM1* transcription in advanced CRC cells remains unclear. Notably, we also observed that ACVR1C expression was markedly upregulated in stage IV CRC (Fig. S3D, E), coinciding with the emergence of epithelial GREM1 expression, whereas stromal GREM1 was already abundantly present in both stage III and IV tumors (Fig. 1B, c and Fig. S2D, E). This spatiotemporal concordance suggests that epithelial GREM1 induction may depend on elevated ACVR1C expression. To investigate the role of the ACVR1C-SMAD2/3 pathway in the exogenous GREM1-mediated tumor *GREM1* transcription, we either overexpressed ACVR1C or inhibited the pathway using SB505124 in SW480 cells following rhGREM1 treatment. Interestingly, ACVR1C overexpression further enhanced endogenous *GREM1* expression, whereas SB505124 treatment completely reversed the effect of rhGREM1 (Fig. 4D). To investigate whether SMAD2/3/4 act as transcription factors for *GREM1*, we utilized the JASPAR database and identified five candidate SMAD2/3/4 binding sites (-733, -612, -446, -316, and -3) in the *GREM1* promoter region (Fig. 4E). To validate the predicted results, we performed a ChIP–qPCR analysis, which revealed that SMAD2/3/4 bound the *GREM1* promoter at the -733 and -612 sites. Notably, SB505124 treatment significantly reduced this binding (Fig. 4F). These data demonstrate that exogenous GREM1 efficiently induces endogenous *GREM1* transcription in CRC cells via the ACVR1C-SMAD2/3 signaling pathway.

Having established that exogenous GREM1 promotes EMT in CRC cells, we sought to determine whether endogenous GREM1 exerts a similar function. In normal epithelial cells, β-CAT is localized at the cellular membrane with the adhesion molecule E-CAD(*40*). However, during tumor progression and the onset of EMT, E-CAD is gradually lost, and a portion of β-CAT translocates to the cytoplasm and nucleus(*41, 42*). To delineate the bona fide correlation between epithelial GREM1 expression and EMT hallmarks in CRC, we performed immunofluorescence (IF) staining on stage IV CRC clinical samples, which contained both GREM1$^+$ and GREM1$^-$ CRC cells. Remarkably, GREM1$^+$ CRC cells exhibited a significant loss of E-CAD, along with increased β-CAT expression and its translocation to the cytoplasm

and nucleus, compared to adjacent GREM1^{-} counterparts within the same tumor (Fig. 4G–J).

We previously found that forced *GREM1* expression (pLV-GREM1) in CRC cells enhanced their EMT and metastatic traits(*20*). Given the typically low expression of GREM1 in CRC cell lines compared to normal and tumoral fibroblasts (Fig. 4K), we sought to model the therapeutic blockade of endogenous GREM1 in advanced tumors. To this end, we used CRISPR/Cas9 techniques to knock out *GREM1* in SW480 and HCT116 cells that stably expressed pLV-GREM1. RT–qPCR analysis revealed that pLV-GREM1 resulted in a significant change in EMT markers, including a marked decrease in *CDH1* and an increase in *SNAI1, VIM,* and *ZEB1,* while *GREM1* knockout significantly restored the expression of these markers, indicating that endogenous GREM1 promotes EMT within CRC cells (Fig. 4L, M). Collectively, these data demonstrate that exogenous GREM1 induces endogenous *GREM1* transcription in CRC cells through the ACVR1C–SMAD2/3 pathway, establishing a self-propelling loop that promotes EMT. Given our observation of a reduction in GREM1 stromal cells in stage IV CRC compared to stage III (Fig. 1B), we speculate that this self-sustaining GREM1 feedback loop enables CRC cells to maintain EMT independently of stromal inputs, reducing their reliance on stromal GREM1. This autonomous signaling cascade comprises multiple nodes that may be amenable to therapeutic intervention aimed at halting CRC metastasis.

Targeting the GREM1-ACVR1C axis to inhibit EMT and metastasis of CRC *in vivo*

To validate the GREM1-ACVR1C-induced autocrine GREM1 feedback loop, we applied genetic and pharmacological strategies (Fig. S6I). First, we evaluated the impact of stromal paracrine GREM1 on CRC *in vivo*. To block exogenous GREM1, we crossed *Grem1-CreER^{T2};Rosa-LSL-DTA* mice with *APC$^{Min/+}$* mice(*43*), a well-established model for CRC proliferation and EMT that develops intestinal tumors by 10 weeks(*41, 44, 45*), generating AGD mice for TMX-induced depletion of GREM1^{+} stromal cells (Fig. 5A). Intriguingly, ablation of Grem1^{+} stromal cells for 6 weeks postnatally did not significantly alter the number or size of intestinal tumors in *APC$^{Min/+}$* mice (Fig. S7A, B). Subsequently, we delved deeper into whether loss of paracrine GREM1 could restrain the malignant potential of intestinal tumor cells. As expected, IF staining in the GREM1^{+} stromal cell infiltration zone of the *APC$^{Min/+}$* intestines revealed a marked loss of E-cad in tumor cells (Fig. 5B, upper left panels), accompanied by increased β-cat expression and its translocation to the cytoplasm and nucleus (Fig. 5B, upper right panels). In contrast, upon depletion of GREM1^{+} stromal cells in AGD mice, E-cad expression was significantly elevated (Fig. 5C), with intense and continuous localization along the tumor cell membrane (Fig. 5B, bottom left). In parallel, β-cat staining was reduced and restricted to the cell membrane (Fig. 5D, E), co-localizing with E-cad, and rarely observed in the cytoplasm or nucleus (Fig.

5B, bottom right panels). These results suggest a critical role for exogenous Grem1 in orchestrating malignant cell behaviors. Next, to evaluate the impact of paracrine Grem1 on CRC metastasis, we injected luciferase-labeled murine rectal cancer cells (MC38-luc) into Grem1^{+} cell-depleted (GD) or control mice (Fig. S7C, D). Cells were administered via the tail vein to induce lung metastasis, or into the spleen or cecum wall to induce liver metastasis(*46*) (Fig. S7E–G). Strikingly, we observed a significant reduction in lung and liver metastases of CRC cells in GD mice compared with *Grem1-CreER*^{T2} or *Rosa-LSL-DTA* controls (Fig. 5F, G, Fig. S7H–K), suggesting that the stromal factor Grem1 is vital for CRC metastasis.

To determine the role of ACVR1C and its downstream SMAD2/3 pathway in GREM1-mediated EMT *in vivo*, we first pre-treated HCT116 cells carrying a luciferase reporter (HCT116-luc), stably expressing either shACVR1C or scramble shRNA, with GREM1-CM, followed by subcutaneous transplantation into nude mice. Notably, ACVR1C knockdown significantly inhibited subcutaneous tumor growth (Fig. S8A–C), accompanied by a significant increase in epithelial gene expression (e.g. *CDH1*) and a marked decrease in mesenchymal gene expression (e.g. *SNAI1*, *CTNNB1*, and *ZEB1*), as shown by RT–qPCR analysis (Fig. S8D). These findings were further corroborated by IF staining of EMT markers, including E-CAD and SNAIL (Fig. S8E–G). Meanwhile, we also harnessed SB505124 as a pharmacological alternative to knock down ACVR1C. Consistent with the genetic approach, SB505124 treatment yielded similar effects on local tumor progression, further substantiating the contextual role of the ACVR1C-SMAD2/3 pathway (Fig. S9A–G). Importantly, to investigate the impact of the ACVR1C-SMAD2/3 axis on metastasis, we injected GREM1-CM-pre-treated HCT116-luc cells, stably expressing either shACVR1C or scramble shRNA, into the tail vein of nude mice. Remarkably, lung metastasis was profoundly suppressed in the *ACVR1C* knockdown group compared with controls (Fig. 5H, Fig. S8H). In parallel, we inoculated GREM1-CM-pre-treated HCT116-luc cells into the cecum wall of NOG (NOD/Shi-scid/IL-2Rγ) mice, a new generation of severely immunodeficient mice(*47*). We found that SB505124 treatment resulted in a significant reduction in liver metastasis (Fig. 5I, Fig. S9H). Collectively, these findings establish the ACVR1C-SMAD2/3 axis as a critical effector of stroma-derived GREM1, and reveal that its inhibition provides an effective strategy to counteract GREM1-induced EMT and metastasis in CRC *in vivo*.

Further, to examine the contribution of tumor-autocrine GREM1 to EMT and metastasis of CRC *in vivo*, we first inoculated HCT116 cells carrying pLV-GREM1 into nude mice, which led to significantly enhanced subcutaneous tumor growth (Fig. S10A–C). Subsequent RT–qPCR analysis demonstrated that autocrine GREM1 upregulated *SNAI1*, *VIM*, and *ZEB1* while downregulating *CDH1* (Fig. S10D). These findings were confirmed by IF staining for EMT markers, including E-CAD and SNAIL (Fig. S10E–G), supporting that autocrine GREM1 enhances the EMT process in CRC cells. Next, to confirm the role of tumoral GREM1 in enhancing CRC

metastasis, we conducted metastasis assays by injecting HCT116-luc cells expressing either pLV-GREM1 or the control vector via the tail vein or into the cecum wall. We found that overexpression of tumoral GREM1 resulted in a significant increase in lung and liver metastasis compared with controls (Fig. 5J, K, Fig. S10H, I). In summary, these findings demonstrate that tumoral GREM1 promotes both EMT and metastasis of CRC cells *in vivo*.

Targeting the GREM1-ACVR1C interaction interface to inhibit metastasis of CRC *in vivo*

In clinical research, the molecular complexity and shared signaling of CRC limit the effective targeted therapy. While the TGFβ superfamily is a promising therapeutic axis(*48*), its intertwined and overarching roles in development and physiology make selective targeting difficult without systemic toxicity(*49, 50*). Targeting protein–protein interaction (PPI) interfaces is thought to further enhance specificity and reduce off-target effects(*51*). Our investigation of the GREM1-ACVR1C interaction unveiled a potential avenue to overcome these limitations. Based on the principle of interface disruption, we designed a peptide inhibitor derived from amino acid residues 84-102 (AA84-102) of ACVR1C (hereafter referred to as the ACVR1C peptide). We further examined the binding affinity between GREM1 and the ACVR1C peptide using MST. We found that GREM1 exhibited an affinity for the ACVR1C peptide comparable to that for the ACVR1C-ECD (K_d = 92.30 ± 7.51 nM) (Fig. S10J). Pull-down assays showed that the introduction of ACVR1C peptide significantly blocked the GREM1-ACVR1C binding (Fig. 5L, M), suggesting that the peptide disrupts the GREM1-ACVR1C interaction by potently and competitively binding to GREM1. Further, we employed a spleen-to-liver metastasis model to evaluate the functional effect of the ACVR1C peptide in CRC metastasis. Notably, administration of the ACVR1C peptide effectively suppressed the increase in liver metastasis induced by tumor-specific GREM1 overexpression (Fig. 5N and Fig. S10K), suggesting that our ACVR1C peptide significantly attenuated CRC progression by blocking the metastasis-promoting effects of tumor-autonomous autocrine GREM1-ACVR1C signaling, laying the foundation for the development of a novel class of peptide-based targeted therapies in CRC.

Discussion

Whether tumor cells can internalize stromal paracrine signals and convert them into autocrine loops during metastasis has remained unclear. Here, we show that in advanced colorectal cancer, GREM1 undergoes a stromal-to-epithelial shunt and binds ACVR1C to activate SMAD2/3, inducing both *SNAI1* and *GREM1* expression. This establishes a self-amplifying autocrine circuit that drives EMT, conferring signaling autonomy and promoting metastasis. A functional peptide we designed for

targeting the GREM1–ACVR1C interface effectively disrupts this loop and demonstrates therapeutic potential.

Intercellular communication during embryonic development, tissue repair, and tumor progression is critically orchestrated by secreted signaling molecules, particularly through paracrine and autocrine mechanisms that govern cell fate and behavior(*52*). For instance, factors such as IGF-I and IL-24 coordinate cellular proliferation, differentiation, and microenvironmental remodeling in skeletal development and skin wound healing via both paracrine and autocrine routes(*53, 54*). Similarly, tumor cells exploit these dual signaling modes to enhance their survival and invasive capacity(*55*). During dissemination to distant sites, metastatic tumor cells have been observed to bring along components of the primary tumor stroma, including CAFs, reflecting their persistent reliance on microenvironmental support(*7, 56*). In the seminal work on TGF, Sporn et al. first proposed that a potential mechanism of malignant transformation involves the autocrine production of growth factors to which the cell itself is responsive, thereby enabling escape from microenvironmental dependence. This mechanism may represent an evolutionary reactivation of autocrine strategies utilized during early embryonic development, allowing cells to maintain survival even in the absence of external support(*57, 58*). Weinberg et al. further suggested that paracrine signals from the stroma might trigger the emergence of signaling autonomy in tumor cells. Yet, the exact pathways by which such a shift toward autocrine self-sufficiency is achieved have not been conclusively elucidated(*9*). While neuron-secreted NLGN3 has been reported to upregulate NLGN3 expression in glioma cells, it has not been demonstrated whether this process evolves into a self-sustaining autocrine loop (*59*). Thus, whether tumor cells can transition from paracrine induction to a self-sustaining autocrine circuit, and thereby maintain their malignant phenotype in the absence of the native microenvironment, remains an unresolved question. In this study, we show that during CRC metastasis, GREM1 expression undergoes a stromal-to-epithelial shunt, establishing an autocrine signaling mode initiated by paracrine cues. This transition suggests that metastatic cells acquire signaling autonomy by reactivating developmental autocrine programs, enabling them to survive and disseminate in distant organs with reduced microenvironmental support. Such a shift from “dependence on soil” to “self-construction of soil” reflects the remarkable adaptability of tumor cells and represents a pivotal step in the evolution of metastatic competence.

As a canonical antagonist of BMPs within the TGF-β superfamily, GREM1 plays a pivotal regulatory role across diverse physiological and pathological contexts. During embryogenesis, GREM1 modulates BMP gradients to orchestrate the development of organs such as the kidney(*60*), skeleton(*25*), and limbs(*61*), and is particularly essential for maintaining mesenchymal stemness and tissue integrity in the gut(*25*). Beyond development, GREM1-mediated BMP signaling is also critically involved in benign conditions including obesity(*62*), tissue repair(*63*), and fibrosis(*64*). In the

context of cancer, GREM1 displays marked tissue-specific functionality. In intestinal tumors, studies led by Tomlinson's group and collaborators revealed that in hereditary mixed polyposis syndrome (HMPS), duplication of an upstream enhancer drives aberrant GREM1 expression in epithelial cells, disrupting the BMP-driven stemness gradient and expanding progenitor-like cells toward the mucosal surface, thereby initiating polyp development(*65-67*). GREM1 also reinforces stemness and tumor progression by suppressing BMP signaling in colorectal cancer(*13*). In contrast, in pancreatic ductal adenocarcinoma, GREM1 expression constrains EMT and promotes differentiation toward a less invasive epithelial phenotype(*17*). While traditionally categorized as a BMP antagonist, portraying GREM1 solely as an inhibitory molecule overlooks its diverse and at times paradoxical roles in various biological settings(*68*). Accumulating evidence suggests that GREM1 possesses non-canonical, BMP-independent activities, engaging multiple receptors and activating diverse downstream signaling pathways. Previous studies have implicated EGFR(*69*) and VEGFR2(*23*) as putative GREM1 targets, though their binding affinities have not been determined. Zhu et al. reported that GREM1 binds to FGFR1 with a dissociation constant of K_d = 10.6 nM(*18*). In this study, we further identified ACVR1C(*70*) as a novel binding receptor for GREM1, with a dissociation constant of K_d = 67.67 ± 10.35 nM. Notably, this binding affinity is markedly higher than that of the canonical ACVR1C ligand Activin B (K_d = 854.1 ± 127.47 nM), representing a 12.6-fold increase. These results suggest that GREM1 engages ACVR1C with superior affinity, indicating its potential to act as a dominant ligand within this signaling pathway.

Unlike the mechanism described by Lan et al. in pancreatic cancer, where GREM1 inhibits EMT via classical BMP antagonism, our findings demonstrate that GREM1 binds ACVR1C and activates the SMAD2/3 axis independently of BMP signaling. This interaction initiates a positive autocrine feedback loop that promotes EMT and metastasis in CRC. These contrasting roles highlight the context-dependent plasticity of GREM1, which may engage distinct signaling programs across tissue types to drive divergent cellular outcomes. While GREM1 has not been systematically recognized as a member of the cytokine family, emerging evidence suggests it acts as an adipokine in adipose tissue, modulating metabolic homeostasis(*71*). Our study extends this concept by showing that GREM1 exhibits key cytokine characteristics, including active secretion, receptor engagement, downstream signaling activation, and autocrine feedback amplification. Reframing GREM1 as a cytokine beyond BMP antagonism may provide new insights into its pleiotropic roles in cancer, metabolic disorders, and developmental or regenerative processes.

The rise of cancer genomics and precision medicine has ushered in a new era of molecularly tailored therapies for advanced CRC. Approved targeted agents, including those against VEGF, EGFR, BRAF V600E mutations, and HER2 alterations, have shown efficacy in genetically defined patient subsets(*72*). Yet, challenges such as limited bioavailability, acquired resistance, and narrow indications constrain their

widespread utility(*73*). Distinct from mutation-restricted targets, GREM1 is a broadly expressed cytokine with sustained activity across diverse pathological stages. Its tractable biology and context-specific signaling functions highlight GREM1 as an attractive, potentially more universally applicable therapeutic target in CRC. Therapeutic targeting of GREM1 to date has focused largely on full neutralization strategies using monoclonal antibodies. Fully humanized monoclonal antibodies such as Ginisortamab and TST003 have advanced into phase I/II clinical trials(*74-77*). Although these antibodies have shown efficacy in preclinical models, the indispensable roles of GREM1 in physiological processes such as intestinal homeostasis and bone marrow hematopoiesis raise the risk of adverse effects from systemic inhibition, posing a major challenge to their clinical translation(*63, 78*). In recent years, PPIs have evolved from being considered "undruggable" to emerging as attractive therapeutic targets. Among strategies to modulate PPIs, small peptides have demonstrated particular promise due to their high binding affinity and specificity(*79*). In this study, we propose a more selective therapeutic strategy by leveraging the structural interface of the GREM1–ACVR1C interaction. Using structure-guided molecular design, we developed a high-affinity peptide that specifically disrupts this interaction in tumor cells, leading to a marked inhibition of metastatic potential. Unlike conventional neutralizing antibodies that globally suppress GREM1 activity, our approach targets the pathogenic GREM1–ACVR1C axis with precision, offering a highly selective therapeutic avenue for metastatic CRC. This work highlights the translational potential of targeting PPIs as an anticancer strategy through rational molecular intervention.

In summary, our findings reveal that the GREM1–ACVR1C axis acts as a key mediator of the stromal-to-epithelial shunt and the establishment of autonomous GREM1 signaling in CRC. By uncovering this pathway, we not only deepen our understanding of tumor self-sufficiency mechanisms, but also identify a functionally precise intervention point that opens new avenues for disrupting metastatic competence through targeted dismantling of self-reinforcing oncogenic circuits.

References

1. A. Canellas-Socias, E. Sancho, E. Batlle, Mechanisms of metastatic colorectal cancer. *Nat Rev Gastroenterol Hepatol* **21**, 609-625 (2024).
2. I. Pastushenko, C. Blanpain, EMT Transition States during Tumor Progression and Metastasis. *Trends in cell biology* **29**, 212-226 (2019).
3. K. E. de Visser, J. A. Joyce, The evolving tumor microenvironment: From cancer initiation to metastatic outgrowth. *Cancer cell* **41**, 374-403 (2023).
4. M. Song *et al.*, Cancer-Associated Fibroblast-Mediated Cellular Crosstalk Supports Hepatocellular Carcinoma Progression. *Hepatology* **73**, 1717-1735 (2021).
5. K. Nee *et al.*, Preneoplastic stromal cells promote BRCA1-mediated breast tumorigenesis. *Nature genetics* **55**, 595-606 (2023).
6. J. Tommelein *et al.*, Radiotherapy-Activated Cancer-Associated Fibroblasts Promote Tumor Progression through Paracrine IGF1R Activation. *Cancer Res* **78**, 659-670 (2018).
7. P. Hurtado, I. Martinez-Pena, R. Pineiro, Dangerous Liaisons: Circulating Tumor Cells (CTCs) and Cancer-Associated Fibroblasts (CAFs). *Cancers (Basel)* **12**, (2020).
8. A. W. Lambert, Y. Zhang, R. A. Weinberg, Cell-intrinsic and microenvironmental determinants of metastatic colonization. *Nat Cell Biol* **26**, 687-697 (2024).
9. D. Hanahan, R. A. Weinberg, The hallmarks of cancer. *Cell* **100**, 57-70 (2000).
10. L. Cords, N. de Souza, B. Bodenmiller, Classifying cancer-associated fibroblasts-The good, the bad, and the target. *Cancer cell* **42**, 1480-1485 (2024).
11. Y. Chen, K. M. McAndrews, R. Kalluri, Clinical and therapeutic relevance of cancer-

630 associated fibroblasts. *Nat Rev Clin Oncol* **18**, 792-804 (2021).

631 12. H. Luo *et al.*, Pan-cancer single-cell analysis reveals the heterogeneity and plasticity
632 of cancer-associated fibroblasts in the tumor microenvironment. *Nat Commun* **13**,
633 6619 (2022).

634 13. H. Kobayashi *et al.*, The Balance of Stromal BMP Signaling Mediated by GREM1 and
635 ISLR Drives Colorectal Carcinogenesis. *Gastroenterology* **160**, 1224-1239 e1230
636 (2021).

637 14. T. Li *et al.*, Over-expressed Phospholamban in Cancer-associated Fibroblasts Is a
638 Driver for CMS4 Subtype Colorectal Cancer Formation. *Cell Mol Gastroenterol*
639 *Hepatol* **19**, 101524 (2025).

640 15. Y. Jiang *et al.*, Mapping and tracing Grem1(+) stromal cells in an Apc (Min/+) mouse
641 utilizing cryopreserved intestinal sections prepared via modified Swiss-roll technique.
642 *iScience* **27**, 111173 (2024).

643 16. J. Ren *et al.*, Cancer-associated fibroblast-derived Gremlin 1 promotes breast cancer
644 progression. *Breast Cancer Res* **21**, 109 (2019).

645 17. L. Lan *et al.*, GREM1 is required to maintain cellular heterogeneity in pancreatic
646 cancer. *Nature* **607**, 163-168 (2022).

647 18. C. Cheng *et al.*, Gremlin1 is a therapeutically targetable FGFR1 ligand that regulates
648 lineage plasticity and castration resistance in prostate cancer. *Nat Cancer* **3**, 565-580
649 (2022).

650 19. E. Jaeger *et al.*, Hereditary mixed polyposis syndrome is caused by a 40-kb upstream

651 duplication that leads to increased and ectopic expression of the BMP antagonist
652 GREM1. *Nature genetics* **44**, 699-703 (2012).
653 20. R. Li *et al.*, Gremlin-1 Promotes Colorectal Cancer Cell Metastasis by Activating
654 ATF6 and Inhibiting ATF4 Pathways. *Cells* **11**, (2022).
655 21. Y. Liu, Y. Li, R. Hou, Z. Shu, Knockdown GREM1 suppresses cell growth,
656 angiogenesis, and epithelial-mesenchymal transition in colon cancer. *Journal of*
657 *cellular biochemistry* **120**, 5583-5596 (2019).
658 22. D. P. Brazil, R. H. Church, S. Surae, C. Godson, F. Martin, BMP signalling: agony
659 and antagony in the family. *Trends in cell biology* **25**, 249-264 (2015).
660 23. S. Mitola *et al.*, Gremlin is a novel agonist of the major proangiogenic receptor
661 VEGFR2. *Blood* **116**, 3677-3680 (2010).
662 24. S. A. Park *et al.*, Gremlin-1 augments the oestrogen-related receptor alpha signalling
663 through EGFR activation: implications for the progression of breast cancer. *Br J*
664 *Cancer* **123**, 988-999 (2020).
665 25. D. L. Worthley *et al.*, Gremlin 1 identifies a skeletal stem cell with bone, cartilage, and
666 reticular stromal potential. *Cell* **160**, 269-284 (2015).
667 26. R. Kalluri, M. Zeisberg, Fibroblasts in cancer. *Nat Rev Cancer* **6**, 392-401 (2006).
668 27. I. Pastushenko *et al.*, Identification of the tumour transition states occurring during
669 EMT. *Nature* **556**, 463-468 (2018).
670 28. H. Zhao *et al.*, Wnt signaling in colorectal cancer: pathogenic role and therapeutic
671 target. *Mol Cancer* **21**, 144 (2022).

672 29. K. Tsuchida *et al.*, Activin isoforms signal through type I receptor serine/threonine
673 kinase ALK7. *Molecular and cellular endocrinology* **220**, 59-65 (2004).
674 30. M. Kisonaite, X. Wang, M. Hyvonen, Structure of Gremlin-1 and analysis of its
675 interaction with BMP-2. *The Biochemical journal* **473**, 1593-1604 (2016).
676 31. R. Derynck, Y. E. Zhang, Smad-dependent and Smad-independent pathways in TGF-
677 beta family signalling. *Nature* **425**, 577-584 (2003).
678 32. A. Dongre, R. A. Weinberg, New insights into the mechanisms of epithelial-
679 mesenchymal transition and implications for cancer. *Nat Rev Mol Cell Biol* **20**, 69-84
680 (2019).
681 33. M. P. Stemmler, R. L. Eccles, S. Brabletz, T. Brabletz, Non-redundant functions of
682 EMT transcription factors. *Nat Cell Biol* **21**, 102-112 (2019).
683 34. S. T. J. Bradford, E. J. Ranghini, E. Grimley, P. H. Lee, G. R. Dressler, High-
684 throughput screens for agonists of bone morphogenetic protein (BMP) signaling
685 identify potent benzoxazole compounds. *The Journal of biological chemistry* **294**,
686 3125-3136 (2019).
687 35. S. DaCosta Byfield, C. Major, N. J. Laping, A. B. Roberts, SB-505124 is a selective
688 inhibitor of transforming growth factor-beta type I receptors ALK4, ALK5, and ALK7.
689 *Molecular pharmacology* **65**, 744-752 (2004).
690 36. Y. Shi, J. Massagué, Mechanisms of TGF-beta signaling from cell membrane to the
691 nucleus. *Cell* **113**, 685-700 (2003).
692 37. L. Asnaghi *et al.*, ACVR1C/SMAD2 signaling promotes invasion and growth in

693 retinoblastoma. *Oncogene* **38**, 2056-2075 (2019).

694 38. S. Yang *et al.*, SEPHS1 promotes SMAD2/3/4 expression and hepatocellular
695 carcinoma cells invasion. *Exp Hematol Oncol* **10**, 17 (2021).

696 39. J. Cai *et al.*, Tumor-Associated Macrophages Derived TGF-beta□Induced Epithelial
697 to Mesenchymal Transition in Colorectal Cancer Cells through Smad2,3-4/Snail
698 Signaling Pathway. *Cancer Res Treat* **51**, 252-266 (2019).

699 40. H. Clevers, Wnt/beta-catenin signaling in development and disease. *Cell* **127**, 469-
700 480 (2006).

701 41. E. Sánchez-Tilló *et al.*, β-catenin/TCF4 complex induces the epithelial-to-
702 mesenchymal transition (EMT)-activator ZEB1 to regulate tumor invasiveness.
703 *Proceedings of the National Academy of Sciences of the United States of America*
704 **108**, 19204-19209 (2011).

705 42. M. Inomata, A. Ochiai, S. Akimoto, S. Kitano, S. Hirohashi, Alteration of beta-catenin
706 expression in colonic epithelial cells of familial adenomatous polyposis patients.
707 *Cancer Res* **56**, 2213-2217 (1996).

708 43. A. R. Moser, H. C. Pitot, W. F. Dove, A dominant mutation that predisposes to
709 multiple intestinal neoplasia in the mouse. *Science* **247**, 322-324 (1990).

710 44. J. Ren, H. Sui, F. Fang, Q. Li, B. Li, The application of Apc(Min/+) mouse model in
711 colorectal tumor researches. *J Cancer Res Clin Oncol* **145**, 1111-1122 (2019).

712 45. R. Babaei-Jadidi *et al.*, FBXW7 influences murine intestinal homeostasis and cancer,
713 targeting Notch, Jun, and DEK for degradation. *The Journal of experimental medicine*

714 **208**, 295-312 (2011).

715 46. L. Zhang *et al.*, Creatine promotes cancer metastasis through activation of Smad2/3.

716 *Cell metabolism* **33**, 1111-1123.e1114 (2021).

717 47. M. Ito *et al.*, NOD/SCID/gamma(c)(null) mouse: an excellent recipient mouse model

718 for engraftment of human cells. *Blood* **100**, 3175-3182 (2002).

719 48. B. Jung, J. J. Staudacher, D. Beauchamp, Transforming Growth Factor β Superfamily

720 Signaling in Development of Colorectal Cancer. *Gastroenterology* **152**, 36-52 (2017).

721 49. S. Liu, J. Ren, P. Ten Dijke, Targeting TGFβ signal transduction for cancer therapy.

722 *Signal Transduct Target Ther* **6**, 8 (2021).

723 50. D. Peng, M. Fu, M. Wang, Y. Wei, X. Wei, Targeting TGF-β signal transduction for

724 fibrosis and cancer therapy. *Mol Cancer* **21**, 104 (2022).

725 51. A. E. Modell, S. L. Blosser, P. S. Arora, Systematic Targeting of Protein-Protein

726 Interactions. *Trends in pharmacological sciences* **37**, 702-713 (2016).

727 52. Y. Xie *et al.*, FGF/FGFR signaling in health and disease. *Signal Transduct Target*

728 *Ther* **5**, 181 (2020).

729 53. Y. Wang, D. D. Bikle, W. Chang, Autocrine and Paracrine Actions of IGF-I Signaling

730 in Skeletal Development. *Bone Res* **1**, 249-259 (2013).

731 54. S. Liu *et al.*, A tissue injury sensing and repair pathway distinct from host pathogen

732 defense. *Cell* **186**, 2127-2143 e2122 (2023).

733 55. R. Basu, C. L. Boguszewski, J. J. Kopchick, Growth Hormone Action as a Target in

734 Cancer: Significance, Mechanisms, and Possible Therapies. *Endocrine reviews* **46**,

735 224-280 (2025).

736 56. Z. Ao *et al.*, Identification of Cancer-Associated Fibroblasts in Circulating Blood from
737 Patients with Metastatic Breast Cancer. *Cancer Res* **75**, 4681-4687 (2015).

738 57. M. B. Sporn, G. J. Todaro, Autocrine secretion and malignant transformation of cells.
739 *N Engl J Med* **303**, 878-880 (1980).

740 58. E. Wydooghe *et al.*, Autocrine embryotropins revisited: how do embryos
741 communicate with each other in vitro when cultured in groups? *Biological reviews of*
742 *the Cambridge Philosophical Society* **92**, 505-520 (2017).

743 59. H. S. Venkatesh *et al.*, Neuronal Activity Promotes Glioma Growth through
744 Neuroligin-3 Secretion. *Cell* **161**, 803-816 (2015).

745 60. O. Michos *et al.*, Gremlin-mediated BMP antagonism induces the epithelial-
746 mesenchymal feedback signaling controlling metanephric kidney and limb
747 organogenesis. *Development (Cambridge, England)* **131**, 3401-3410 (2004).

748 61. J. Malkmus *et al.*, Spatial regulation by multiple Gremlin1 enhancers provides digit
749 development with cis-regulatory robustness and evolutionary plasticity. *Nature*
750 *communications* **12**, 5557 (2021).

751 62. E. Grillo *et al.*, Role of gremlin-1 in the pathophysiology of the adipose tissues.
752 *Cytokine & growth factor reviews* **69**, 51-60 (2023).

753 63. M. A. J. Koppens *et al.*, Bone Morphogenetic Protein Pathway Antagonism by Grem1
754 Regulates Epithelial Cell Fate in Intestinal Regeneration. *Gastroenterology* **161**, 239-
755 254.e239 (2021).

756 64. R. K. Baboota *et al.*, BMP4 and Gremlin 1 regulate hepatic cell senescence during
757 clinical progression of NAFLD/NASH. *Nature metabolism* **4**, 1007-1021 (2022).
758 65. E. Jaeger *et al.*, Hereditary mixed polyposis syndrome is caused by a 40-kb upstream
759 duplication that leads to increased and ectopic expression of the BMP antagonist
760 GREM1. *Nature genetics* **44**, 699-703 (2012).
761 66. H. Davis *et al.*, Aberrant epithelial GREM1 expression initiates colonic tumorigenesis
762 from cells outside the stem cell niche. *Nature medicine* **21**, 62-70 (2015).
763 67. E. J. Mulholland *et al.*, Epithelial GREMLIN1 disrupts intestinal epithelial-
764 mesenchymal crosstalk to induce a wnt-dependent ectopic stem cell niche through
765 stromal remodelling. *Nature communications* **16**, 5167 (2025).
766 68. Z. Gao, J. M. Houthuijzen, P. Ten Dijke, D. P. Brazil, GREM1 signaling in cancer:
767 tumor promotor and suppressor? *J Cell Commun Signal* **17**, 1517-1526 (2023).
768 69. S. A. Park *et al.*, Gremlin-1 augments the oestrogen-related receptor α signalling
769 through EGFR activation: implications for the progression of breast cancer. *British*
770 *journal of cancer* **123**, 988-999 (2020).
771 70. K. Tsuchida, P. E. Sawchenko, S. Nishikawa, W. W. Vale, Molecular cloning of a
772 novel type I receptor serine/threonine kinase for the TGF beta superfamily from rat
773 brain. *Molecular and cellular neurosciences* **7**, 467-478 (1996).
774 71. S. Hedjazifar *et al.*, The Novel Adipokine Gremlin 1 Antagonizes Insulin Action and Is
775 Increased in Type 2 Diabetes and NAFLD/NASH. *Diabetes* **69**, 331-341 (2020).
776 72. L. H. Biller, D. Schrag, Diagnosis and Treatment of Metastatic Colorectal Cancer: A

777 Review. *Jama* **325**, 669-685 (2021).

778 73. F. Ciardiello *et al.*, Clinical management of metastatic colorectal cancer in the era of
779 precision medicine. *CA: a cancer journal for clinicians* **72**, 372-401 (2022).

780 74. G. C. G. Davies *et al.*, Discovery of ginisortamab, a potent and novel anti-gremlin-1
781 antibody in clinical development for the treatment of cancer. *mAbs* **15**, 2289681
782 (2023).

783 75. D. Sarker *et al.*, Abstract CT094: Phase I dose-escalation study evaluating the safety
784 an d tolerability of ginisortamab (UCB6114), a first-in-class anti-gremli n-1 monoclonal
785 antibody (mAb), as monotherapy in advanced solid tumors. *Cancer Research* **83**,
786 CT094-CT094.

787 76. I. R. Rivera *et al.*, Abstract 5977: A first-in-human, open-label, multi-center phase 1
788 stud y of TST003, a GREM 1 inhibitor, in subjects with locally advanced or metastatic
789 solid tumors. *Cancer Research* **84**, 5977-5977.

790 77. D. Sun *et al.*, Abstract 465: The preclinical characterization of TST003, a first-in-c
791 lass mAb targeting gremlin-1 overexpressed by cancer-associated fibrob lasts and
792 tumor cells. *Cancer Research* **83**, 465-465.

793 78. S. C. Rowan *et al.*, Gremlin 1 depletion in vivo causes severe enteropathy and bone
794 marrow failure. *The Journal of pathology* **251**, 117-122 (2020).

795 79. H. Lu *et al.*, Recent advances in the development of protein-protein interactions
796 modulators: mechanisms and clinical trials. *Signal Transduct Target Ther* **5**, 213
797 (2020).

798 80. D. G. Gibson *et al.*, Enzymatic assembly of DNA molecules up to several hundred
799 kilobases. *Nature methods* **6**, 343-345 (2009).
800 81. S. P. Flanagan, 'Nude', a new hairless gene with pleiotropic effects in the mouse.
801 *Genetical research* **8**, 295-309 (1966).
802 82. M. D. Muzumdar, B. Tasic, K. Miyamichi, L. Li, L. Luo, A global double-fluorescent
803 Cre reporter mouse. *Genesis (New York, N.Y. : 2000)* **45**, 593-605 (2007).
804 83. D. Voehringer, H. E. Liang, R. M. Locksley, Homeostasis and effector function of
805 lymphopenia-induced "memory-like" T cells in constitutively T cell-depleted mice.
806 *Journal of immunology* **180**, 4742-4753 (2008).
807 84. Y. Yan, D. Zhang, P. Zhou, B. Li, S. Y. Huang, HDOCK: a web server for protein-
808 protein and protein-DNA/RNA docking based on a hybrid strategy. *Nucleic acids*
809 *research* **45**, W365-w373 (2017).

Acknowledgements

We thank Ruohan Li and Changxue Li for assisting with IHC data scoring; Guihua Wang for providing the *APC*$^{Min/+}$ mouse line; Pengcheng Bu for assisting with the construction of the cecum to liver metastasis mouse model; Lei Zhou for drawing the GREM1-ACVR1C protein docking; and Xingqiao Xie from the Sample Preparation and Analysis Core Facility of Shenzhen Medical Academy of Research and Translation (SMART) for technical support of MST. This work was supported by grants from the National Natural Science Foundation of China (81874176, 82072766, 32471261), Guangdong Provincial Key Laboratory of Digestive Cancer Research (2021B1212040006), the Sanming Project of Medicine in Shenzhen (SZSM202111005), funding of Shenzhen Clinical Research Center for Gastroenterology (Gastrointestinal Surgery) (LCYSSQ20220823091203008), Guangdong Medical Science and Technology Research Foundation (A2022068), Guangdong Zhujiang Talent Program (2019QN01Y305), Regional Joint Key Project of Guangdong Province (2022B1515120038), and Shenzhen Science and Technology program (JCYJ20220818102018038).

Author contributions

H.Z. and N.L. conceived and designed the study and wrote the manuscript. H.Z. performed most of the experiments and analyses. Q.J. and Y.J. helped with RT-qPCR analysis and clinical tissue IF experiments. Z.F. and Y.Y. helped with subcutaneous tumor IF experiments. Y.Y. assisted with the design and drawing of schematics and mechanistic diagrams. Y.G. assisted with histopathological assessment. N.W. and B.Z. performed ACVR1C-ECD and ACVR1C-ECD-doble-mutant proteins expression and purification. J.L. helped with single-cell RNA-seq data analysis. Z.Z. helped with the establishment of the cecum to liver metastasis mouse model. L.G., Y.Z. (Affiliation 1), Y.H., Y.Z. (Affiliation 7), and J.Z. provided intellectual feedback. Note: Y.Z. (Affiliation 1) and Y.Z. (Affiliation 7) are distinct individuals. S.L. and L.F. assisted with data interpretation and analysis and text proofreading. X.W. helped with CHIP experiments. T.W. helped with RNA-seq data analysis. X.S., T.W., Y.J. and N.L. supervised the study.

Competing interests

Authors declare that they have no competing interests.

Supplementary Materials

Materials and Methods

Figs. S1 to S11

Tables S1 to S2

References (80–84)

Figure legends

Fig. 1. Ectopic expression of GREM1 protein in CRC. (**A**) Representative images of GREM1 immunohistochemical (IHC) staining (Upper) on human primary CRC samples and illustration of GREM1 expression pattern (Lower). The red dashed line separates tumor from adjacent normal area. N: normal areas; T: tumoral areas; S: stromal areas; Red arrow: GREM1^{+} CRC cells. (**B, C**) Quantification of GREM1 stromal cell infiltration (B) and GREM1 expression in cancer cells (C) across stage I–IV primary CRC tissues from Sun Yat-sen University (SYSU). (**D**) Representative immunofluorescence (IF) images of GREM1 and EPCAM staining in stage IV human primary CRC tumors. A white dashed line separates epithelial and mesenchymal cells. White arrow: GREM1^{+} CRC cells. (**E**) Kaplan–Meier survival curves of 106 CRC patients from SYSU stratified by GREM1 levels in cancer cells. Patients were divided into high and low groups based on the cohort median. For B and C, data are mean ± s.e.m. *P* values were calculated using one-way ANOVA with Bonferroni multiple-comparison test (B, C). Significance was determined using a two-sided log-rank test. HR, hazard ratio (E). Scale bars, 20 μm.

Fig. 2. ACVR1C is a novel GREM1 receptor in CRC. (**A**) Proteins extracted from the HCT116 cells transfected with HA-mCherry-tagged-GREM1 were incubated with magnetic beads conjugated with an anti-HA antibody. Bound proteins were eluted and visualized by Coomassie Brilliant Blue staining. A protein band of ~110 kDa was submitted for mass spectrometry (MS). (**B**) The full amino-acid sequence of human ACVR1C. The sequences in blue are the tryptic peptides identified by MS. (**C**) GREM1 coimmunoprecipitates with ACVR1C in HCT116 cells transfected with HA-mCherry-tagged GREM1 expressing plasmids. The bound proteins were immunoprecipitated with an anti-HA antibody and blotted by anti-HA, anti-ACVR1C, and anti-TGFβR1 antibodies. (**D**) ACVR1C coimmunoprecipitates with GREM1 in HCT116 cells transfected with Flag-tagged ACVR1C expressing plasmids. The bound proteins were immunoprecipitated with an anti-Flag antibody and blotted by an anti-GREM1 antibody. (**E**) Confocal microscopy images of GREM1 and ACVR1C in SW480 cells. Scale bars, 1 μm. (**F**) Interaction of purified GREM1 and ACVR1C-ECD protein demonstrated by pull-down experiments. (**G**) Increasing concentrations of recombinant ACVR1C-ECD-Fc protein (0-27.5 μM) were incubated with Red-labeled 50 nM recombinant GREM1-his or ACTIVIN B-his. MST was used to evaluate ACVR1C-ECD-Fc binding to GREM1-his or ACTIVIN B-his (n = 3 independent experiments), data are presented as mean ± s.e.m. (**H, I**) Diagrams of truncated ACVR1C (h, left) and truncated GREM1 (i, left), with corresponding coimmunoprecipitation results (right) comparing truncation mutants with binding partners. (**J**) Molecular docking of GREM1 and ACVR1C-ECD simulated by HDOCK (http://hdock.phys.hust.edu.cn/). Protein structures were generated from PDB (http://www.rcsb.org/, GREM1: 5AEJ) and AlphaFold (http://alphafold.ebi.ac.uk/, ACVR1C: Q8NER5). Docking module highlighting key amino acid residues in the binding pocket between GREM1 and ACVR1C. (**K**)

Schematic of ACVR1C mutations (point mutations highlighted in red, Upper). Coimmunoprecipitation of ACVR1C and GREM1 is impaired by the AA_{85} mutant (M2) or the AA_{101} mutant (M3) of ACVR1C (Lower). (**L**) Schematic of GREM1 mutations (point mutations highlighted in red, Upper). Coimmunoprecipitation of ACVR1C and GREM1 is impaired by the $AA_{100\text{-}102/112/115}$ mutant (M3) of GREM1 (Lower).

Fig. 3. Secretory GREM1 binding of ACVR1C induced EMT via SMAD2/3 pathway. (**A**) RNA sequencing was performed on HCT116 cells treated with GREM1 conditioned medium (GREM1-CM) or control conditioned medium (Vec-CM), followed by GSEA of the C2 gene sets. NES, normalized enrichment score, all P-values equal to 0. (**B**) Activation levels of the ACVR1C pathway markers p-SMAD2/3 and SMAD2/3 and expression of epithelial marker E-CAD, mesenchymal markers SNAIL, ZEB1 and β-CAT were compared by immunoblotting analysis in SW480 and HCT116 cells treated with Vec-CM, GREM1-CM, GREM1-CM + GREM1 BAb or GREM1-CM + IgG. (**C**) Immunoblotting for the ACVR1C pathway markers p-SMAD2/3 and SMAD2/3 and the BMPR pathway markers p-SMAD1/5/9 and SMAD1 and the TGFβR pathway markers TGFβR1 and TGFβ from the lysates of HCT116 or SW480 cells with a concentration gradient of rhGREM1 treatment. (**D**) Schematic representation of the TGFβ signaling pathway, highlighting GREM1-induced activation of ACVR1C and inhibition of BMPR signaling. (**E**) Immunoblotting for the BMPR pathway markers p-SMAD1/5/9 and SMAD1 and expression of epithelial marker E-CAD, mesenchymal markers SNAIL and ZEB1 from the lysates of HCT116 or SW480 cells treated with GREM1-CM and different concentrations of BMP agonist, sb4. (**F**) SW480 and HCT116 cells were transfected with control shRNA (Scramble shRNA) or with one of two ACVR1C-targeting shRNAs (denoted shACVR1C#1 and shACVR1C#2) and separately treated with Vec-CM or GREM1-CM; epithelial marker E-CAD and mesenchymal markers SNAIL and ZEB1 were analyzed by immunoblotting. (**G**) Expression of epithelial markers E-CAD and mesenchymal markers SNAIL, ZEB1 and β-CAT were compared by immunoblotting analysis in SW480 and HCT116 cells treated with Vec-CM, GREM1-CM or GREM1-CM + SB505124 (1 μM). SB505124 inhibits the ACVR1C signaling pathway by impairing SMAD2/3 phosphorylation. CM, culture medium. For p-SMAD2/3, SMAD2/3 was used as a control. For other proteins, β-actin was used as a loading control.

Fig. 4. Secreted GREM1 upregulates *GREM1* transcription via ACVR1C-SMAD2/3 pathway to reinforce EMT in CRC. (A, B) RT–qPCR analysis of *GREM1* mRNA levels in SW480 (A) and HCT116 (B) cells treated with increasing concentrations of rhGREM1. n = 3 biological replicates. (**C**) Immunoblotting of GREM1 protein levels in SW480 and HCT116 cells treated with the concentration gradient of rhGREM1 used in (A) and (B). (**D**) RT–qPCR analysis of *GREM1* expression in SW480 cells treated with rhGREM1 (400 ng/mL). n = 3 biological

replicates. (**E**) SMAD2/3/4 binding motifs in the *GREM1* promoter, predicted by the JASPAR database. Red boxes denote predicted binding sites upstream of the transcription start site (TSS). (**F**) ChIP analysis of p-SMAD2/3 binding sites on the *GREM1* promoter in SW480 cells, treated as indicated. IgG control or SMAD2/3 antibodies were used for ChIP and DNA was quantified by qPCR. DNA levels for each condition were normalized to the input, and the fold-change was calculated over the vehicle control (n = 3 independent experiments). *ns*: not significant. (**G**) Representative IF images for staining of GREM1, E-CAD and β-CAT in stage □ human primary CRC tumors from SYSU. The white square-dashed box in the left image indicates the location of the corresponding region in the right image. The white irregular-dashed box marks the GREM1□ CRC cells, while the brown irregular-dashed box marks the GREM1^{-} CRC cells. Scale bars, 20 μm. (**H, I)** Quantification of the fluorescence intensity of E-CAD (H) and β-CAT (I) between GREM1^{+} and GREM1^{-} CRC subpopulations shown in (G) (n = 3 patients). (**J**) Quantification of the percentage of cells exhibiting cytoplasmic and nuclear translocation of β-CAT in the conditions shown in (G) (n = 3 patients). (**K**) RT–qPCR analysis of *GREM1* mRNA expression levels in CRC cell lines (DLD1, LOVO, HCT116, LS174T, SW480, and HT29), primary fibroblasts (normal fibroblasts and tumoral fibroblasts) derived from the gut of human CRC patients. (**L, M**) RT–qPCR analysis of *GREM1*, epithelial marker *CDH1* and mesenchymal markers *ZEB1* and *VIM* in HCT116 cells infected with control (pLV) or GREM1-overexpressing (pLV-GREM1) lentiviruses or GREM1-overexpressing cells transduced with one of two GREM1-targeting sgRNAs (denoted GREM1KO26 and GREM1KO27), n = 3 independent experiments. For A, B, D, F and H–M, data are presented as mean ± s.e.m. *P* values were calculated using one-way ANOVA with Bonferroni multiple-comparison test (A, B, D, F, L, M) and two-tailed Student's t-test (H–J).

Fig. 5. Targeting the GREM1-ACVR1C axis to inhibit EMT and metastasis of CRC *in vivo*. (**A**) Diagram of the AGD Mouse Model (*APC$^{Min/+}$;Grem1-CreER^{T2};Rosa-LSL-DTA*) and the experimental approach. Grem1□ cells are selectively deleted through tamoxifen (TMX)-induced DTA expression via Cre-lox recombination. Mice received TMX (100 mg/kg) by oral gavage for five consecutive days starting at 4 weeks of age, followed by weekly TMX administration until analysis at 11 weeks. The black triangle indicates the loxP sites. (**B**) Representative IF images of staining for Grem1 and E-cad and β-cat in AGD or control mice (*APC$^{Min/+}$;Grem1-CreER^{T2}* or *APC$^{Min/+}$;Rosa-LSL-DTA*). The white irregular dashed box indicates the infiltrated region of Grem1^{+} stromal cells. Scale bars, 10 μm. (**C, D**) Quantification of the fluorescence intensity of E-cad (C) and β-cat (D) between AGD and control mice shown in (B) (n = 5 mice per group). (**E**) Quantification of the percentage of cells exhibiting cytoplasmic and nuclear translocation of β-cat under the conditions shown in (B) (n = 5 mice per group). (**F**) Diagram of the GD mouse CRC model and the experimental approach. GD and control (*Grem1-CreER^{T2}* or *Rosa-LSL-DTA*) mice received TMX (100 mg/kg) by oral gavage for five consecutive days

starting at 6 weeks of age, followed by weekly doses. At designated time points, MC38-luciferase (MC38-luc) cells were injected intravenously, intrasplenically, or into the cecal wall. Lung and liver metastases were imaged and quantified every five days using the IVIS Lumina Imaging System. The black triangle indicates the loxP sites. (**G**) Quantification of lung and liver metastases. GD or control mice were injected intravenously, intrasplenically, or into the cecum wall with MC38-luc cells. Lung or liver metastases were imaged and quantified by IVIS Lumina Imaging System and quantified (n = 5 mice per group). met., metastases. (**H**) Quantification of the lung metastases. Mice were injected intravenously with HCT116□luciferase (HCT116□luc) cells, which were transduced with Scramble shRNA or shACVR1C and treated with GREM1-CM. Lung metastases were imaged and quantified by IVIS Lumina Imaging System. (**I**) Quantification of liver metastases. The cecum of NOG mice was injected with HCT116□luc cells with GREM1-CM treatment, and mice were treated with SB505124 or a solvent control via abdominal injection. Liver metastases were imaged and quantified by IVIS Lumina Imaging System (n = 5 mice per group). (**J**) Quantification of lung metastases. Mice were injected intravenously with HCT116 cells infected with pLV or pLV-GREM1 lentivirus. Lung tissue sections were stained for Ki67 by IHC, and lung metastases larger than 0.1 mm were counted (n = 5 mice per group). (**K**) Quantification of liver metastases. NOG mice's cecum wall was injected with HCT116□luc cells (pLV/ pLV-GREM1). Liver metastases were imaged and quantified by IVIS Lumina Imaging System (n = 5 mice per group). (**L**) Docking module of GREM1 and ACVR1C-ECD, highlighting key amino acid sequence between GREM1 and ACVR1C (ACVR1C peptide). (**M**) The pull-down assay confirmed that ACVR1C peptide blocked the interaction between GREM1 and ACVR1C-ECD protein. The black arrow indicates the GREM1-his band. (**N**) Quantification of liver metastases. NOG mice's spleen was injected with HCT116□luc cells (pLV/ pLV-GREM1). Treatment was started 48 h after cell injection. ACVR1C peptide was given once every other day (10□mg/kg i.v.). i.v.: intravenous injection. Liver metastases were imaged and quantified by IVIS Lumina Imaging System (n = 5 mice per group). For C–E, G–K, and N, data are presented as mean ± s.e.m. *P* values were calculated using two-tailed Student's t-test (C–E, G, I–K) or one-way ANOVA with Bonferroni multiple-comparison test (H, N).

1010 **Fig. 1**

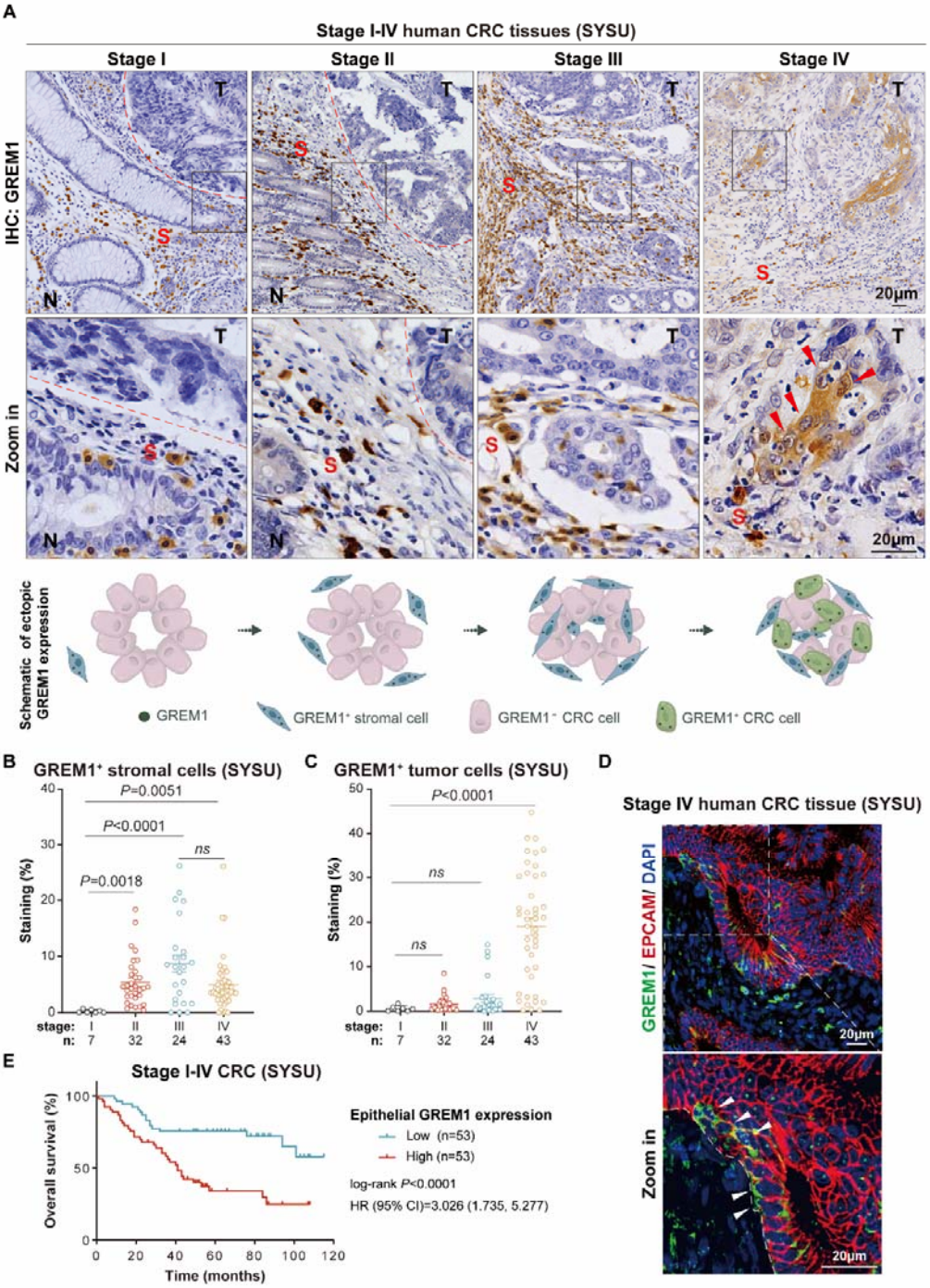

1011

1012

1013 **Fig. 2**

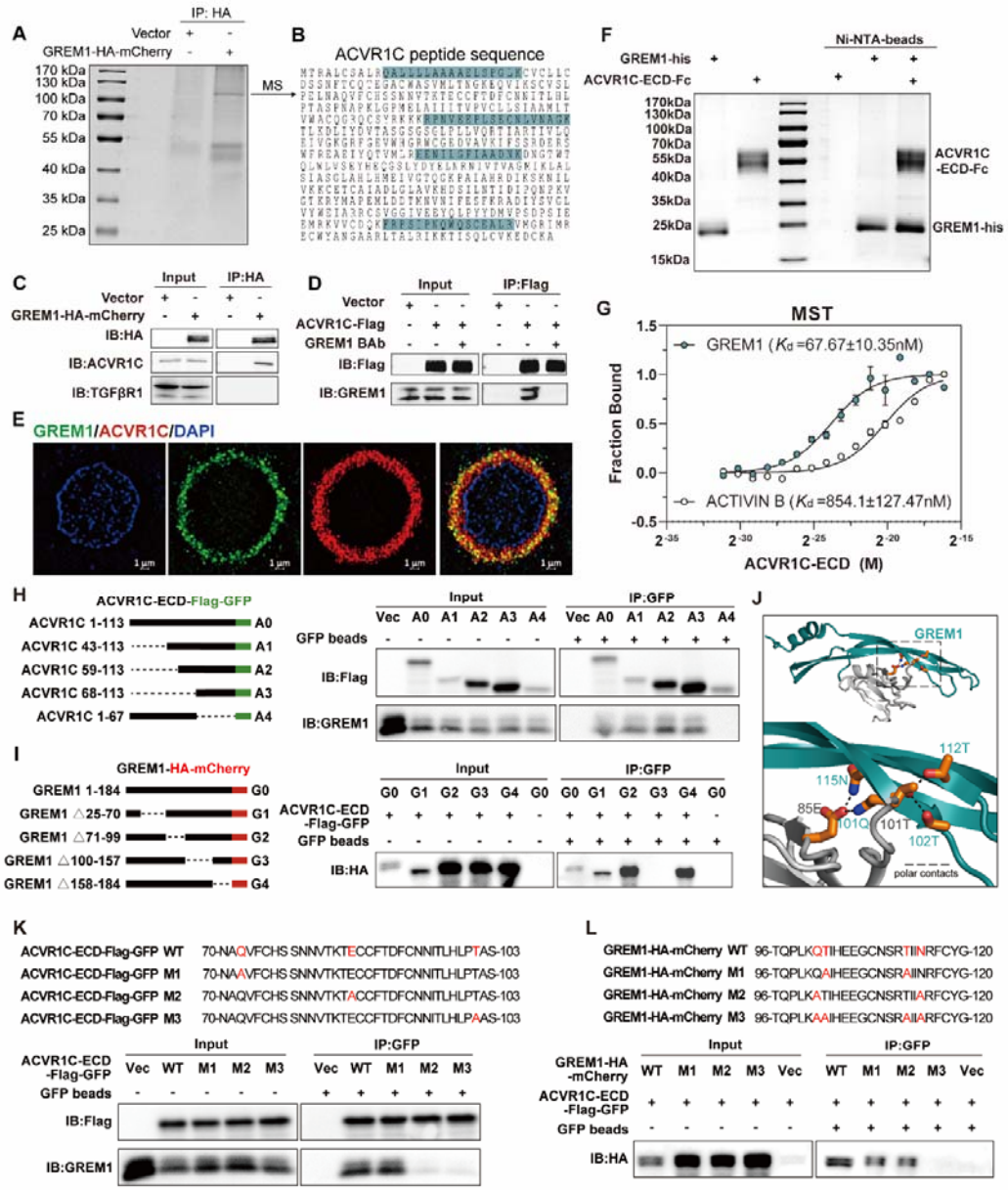

1014

1015

1016 **Fig. 3**

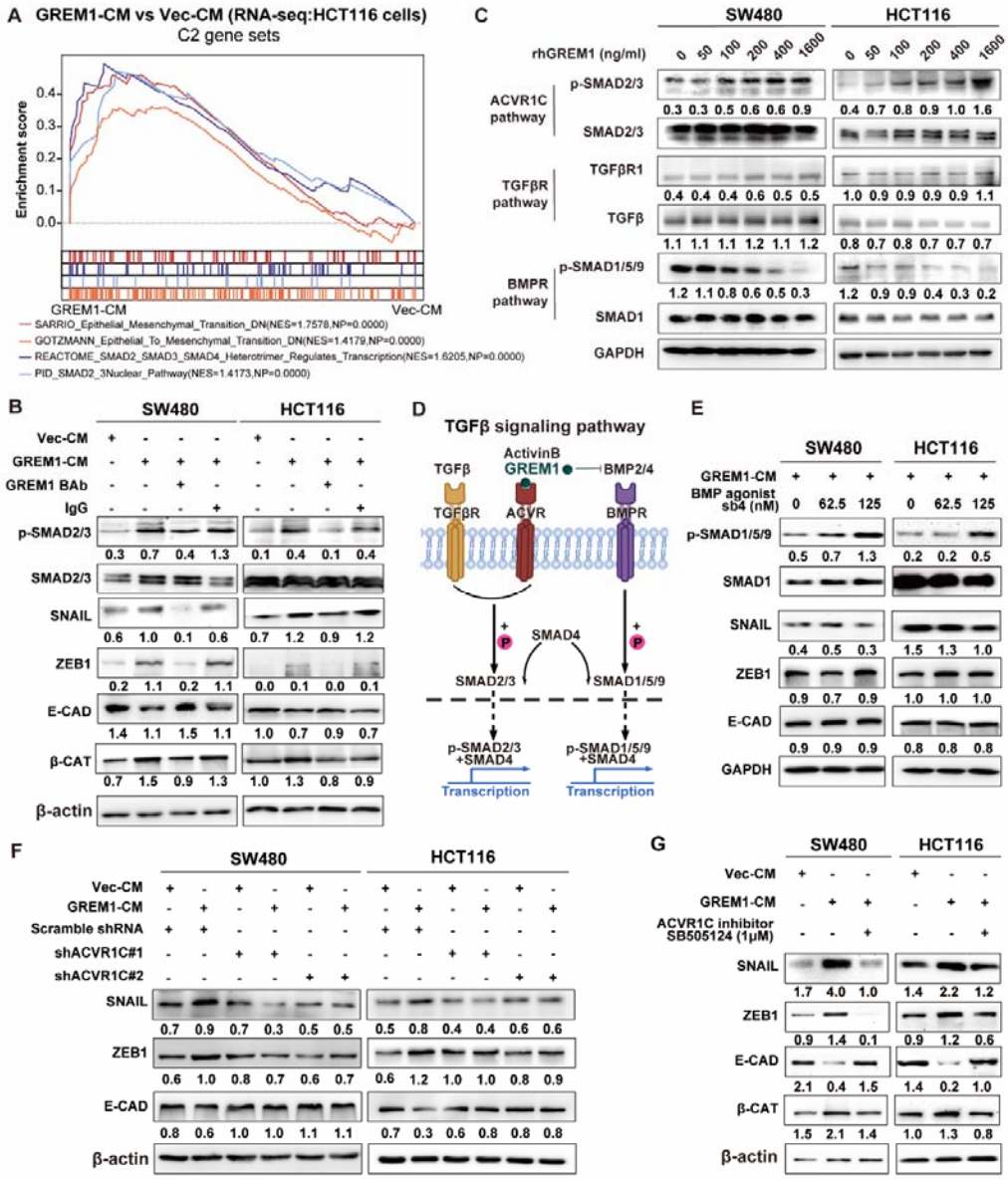

1017
1018

1019 **Fig. 4**

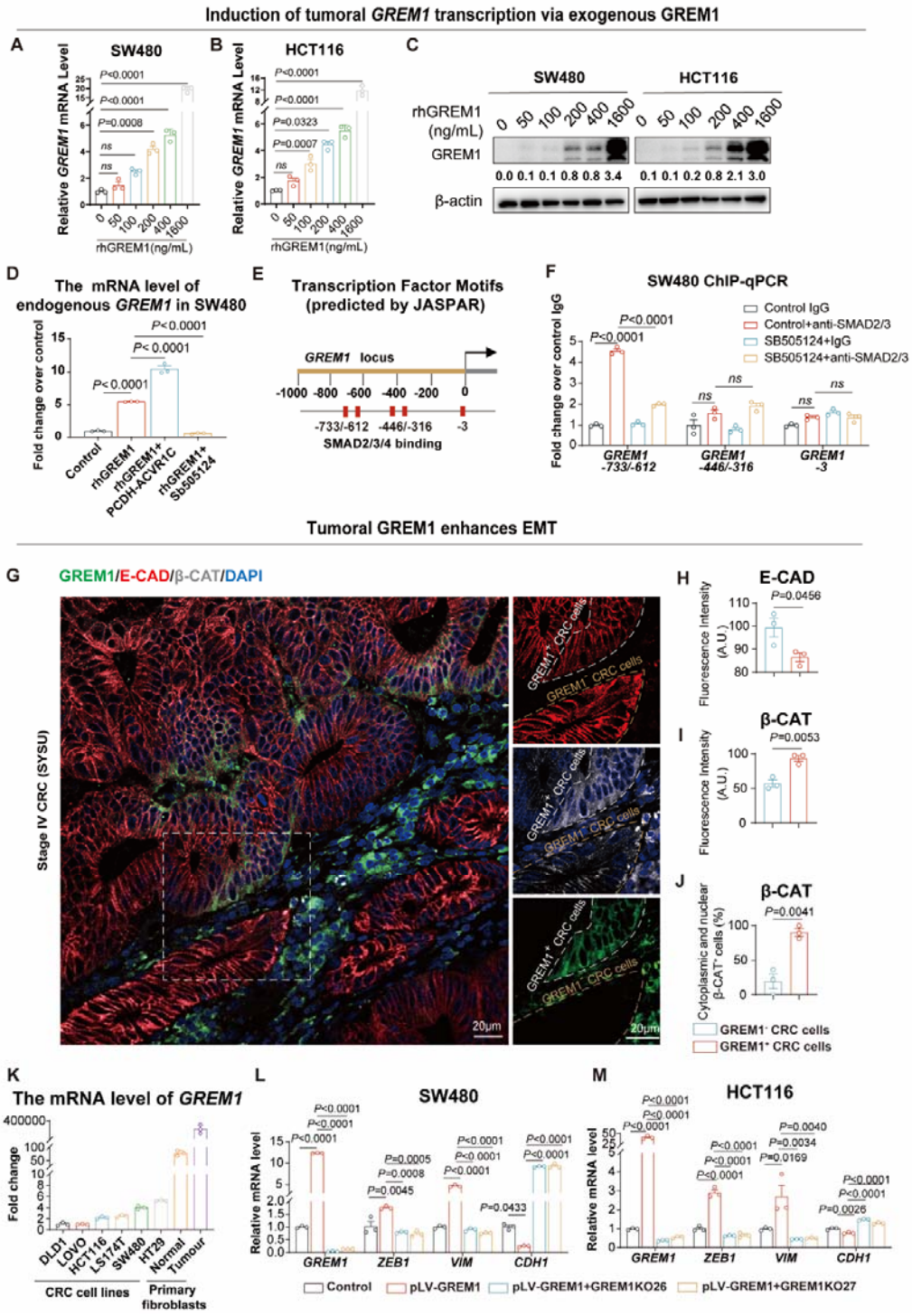

1020

1021

1022 **Fig. 5**

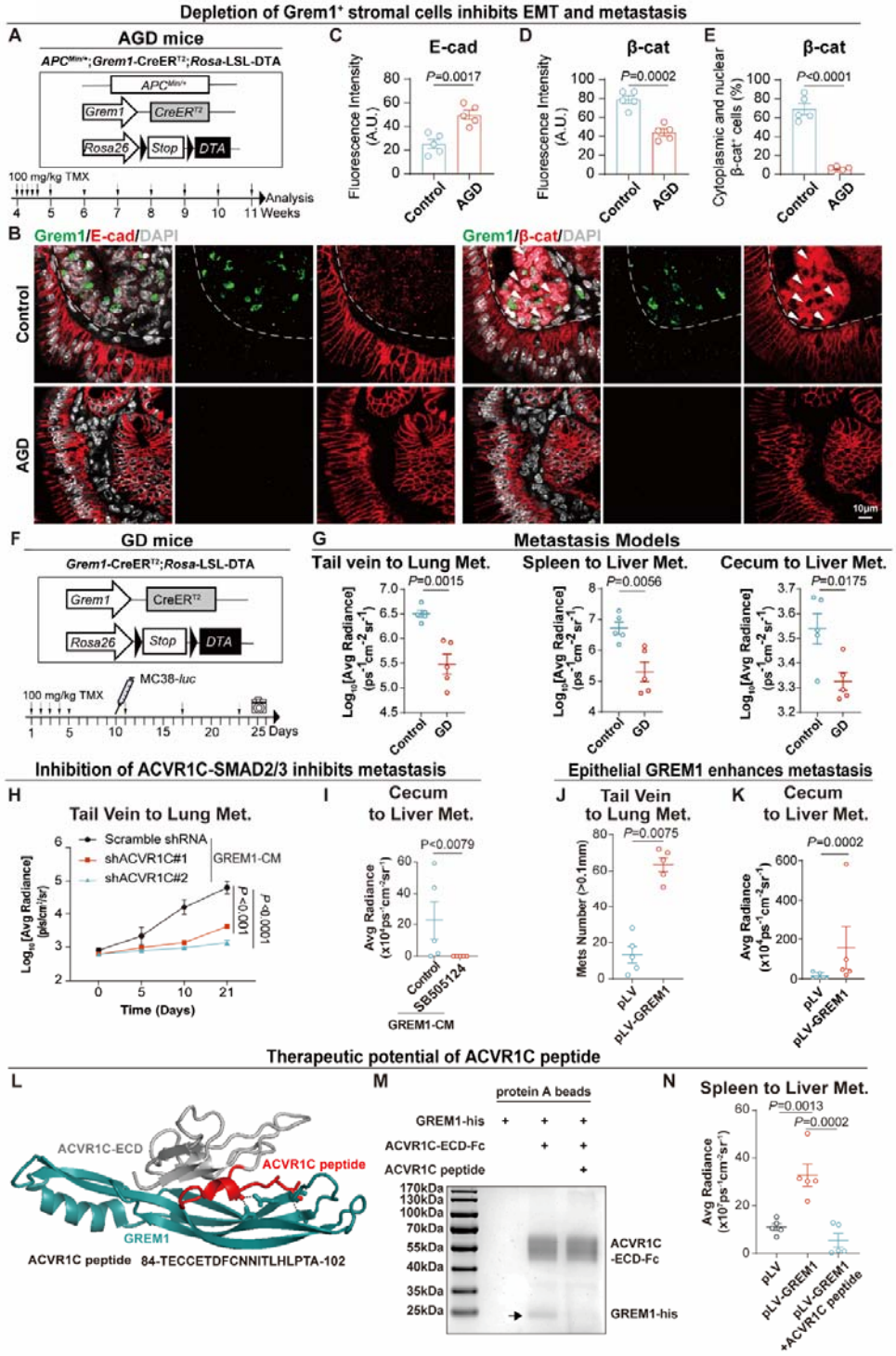

1023